Imaging based optofluidic air flow meter with polymer interferometers defined by soft lithography

Wuzhou Song* and Demetri Psaltis

Optics Laboratory, School of Engineering, Swiss Federal Institute of Technology Lausanne (EPFL), CH-1015 Lausanne, Switzerland
**wuzhou.song@epfl.ch*

Abstract: We present an optofluidic chip with integrated polymer interferometers for measuring both the microfluidic air pressure and flow rate. The chip contains a microfluidic circuit and optical cavities on a polymer which was defined by soft lithography. The pressure can be read out by imaging the interference patterns of the cavities. The air flow rate was then calculated from the differential pressure across a microfluidic Venturi circuit. Air flow rate measurement in the range of 0-2mg/second was demonstrated. This device provides a simple and versatile way for in situ measuring the microscale air pressure and flow on chip.

OCIS codes: (120.5475) Pressure measurement; (120.3180) Interferometry; (350.3950) Micro-optics.

Reference and links

1. D. Psaltis, S. R. Quake, and C. Yang, "Developing optofluidic technology through the fusion of microfluidics and optics," Nature **442**(7101), 381–386 (2006).
2. C. Monat, P. Domachuk, and D. J. Eggleton, "Integrated optofluidics: a new river of light," Nat. Photonics **1**(2), 106–114 (2007).
3. X. Wu, Y. Sun, J. D. Suter, and X. Fan, "Single mode coupled optofluidic ring resonator dye lasers," Appl. Phys. Lett. **94**(24), 241109 (2009).
4. F. B. Arango, M. B. Christiansen, M. Gersborg-Hansen, and A. Kristensen, "Optofluidic tuning of photonic crystal band edge lasers," Appl. Phys. Lett. **91**(22), 223503 (2007).
5. W. Song, A. E. Vasdekis, Z. Li, and D. Psaltis, "Low-order distributed feedback optofluidic dye laser with reduced threshold," Appl. Phys. Lett. **94**(5), 051117 (2009).
6. W. Song, A. E. Vasdekis, Z. Li, and D. Psaltis, "Optofluidic evanescent dye laser based on a distributed feedback circular grating," Appl. Phys. Lett. **94**(16), 161110 (2009).
7. C. Karnutsch, C. C. Smith, A. Graham, S. Tomljenovic-Hanic, R. McPhedran, B. J. Eggleton, L. O'Faolain, T. F. Krauss, S. Xiao, and N. A. Mortensen, "Temperature stabilization of optofluidic photonic crystal cavities," Appl. Phys. Lett. **94**(23), 231114 (2009).
8. A. Groisman, S. Zamek, K. Campbell, L. Pang, U. Levy, and Y. Fainman, "Optofluidic 1x4 switch," Opt. Express **16**(18), 13499–13508 (2008).
9. X. Mao, J. R. Waldeisen, B. K. Juluri, and T. J. Huang, "Hydrodynamically tunable optofluidic cylindrical microlens," Lab Chip **7**(10), 1303–1308 (2007).
10. C. Hilty, E. E. McDonnell, J. Granwehr, K. L. Pierce, S. I. Han, and A. Pines, "Microfluidic gas-flow profiling using remote-detection NMR," Proc. Natl. Acad. Sci. U.S.A. **102**(42), 14960–14963 (2005).
11. D. S. Chang, S. M. Langelier, and M. A. Burns, "An electronic Venturi-based pressure microregulator," Lab Chip **7**(12), 1791–1799 (2007).
12. S. Li, J. C. Day, J. J. Park, C. P. Cadou, and R. Ghodssi, "A fast-response microfluidic gas concentrating device for environmental sensing," Sens. Actuators A Phys. **136**(1), 69–79 (2007).
13. M. Yamada, and M. Seki, "Nanoliter-sized liquid dispenser array for multiple biochemical analysis in microfluidic devices," Anal. Chem. **76**(4), 895–899 (2004).
14. M. A. Unger, H. P. Chou, T. Thorsen, A. Scherer, and S. R. Quake, "Monolithic microfabricated valves and pumps by multilayer soft lithography," Science **288**(5463), 113–116 (2000).
15. W. Song, and D. Psaltis, "Pneumatically tunable optofluidic dye laser," Appl. Phys. Lett. **96**(8), 081101 (2010).
16. Y. Xu, C. Chiu, F. Jiang, Q. Lin, and Y. Tai, "A MEMS multi-sensor chip for gas flow sensing," Sens. Actuators A Phys. **121**, 253–261 (2005).
17. P. Enoksson, G. Stemme, and E. Stemme, "A silicon resonant sensor structure for Coriolis mass-flow measurements," J. Microelectromech. Syst. **6**(2), 119–125 (1997).
18. R. W. Miller, *Flow Measurement Engineering Handbook*, 3rd ed. (McGraw-Hill, 2006).

#129100 - $15.00 USD Received 27 May 2010; revised 8 Jul 2010; accepted 13 Jul 2010; published 22 Jul 2010

1. Introduction

In the past years optofluidic has received substantial attention in both microfluidics and optics. With the development of microtechnology, multiple optofluidic devices have been realized by merging the optics and fluidics synergistically [1,2], such as dye lasers [3–6], tunable photonics crystals [7], optical switches [8] and fluidic lens [9]. In such devices, the optical functional fluids are normally in the liquid form. On the other hand, the gas phase microfluidic devices have also attracted much attention [10–12]. For example, compressed air has become one of the dominated methods to manipulate the liquid analyte for lab-on-a-chip applications, either by pushing the liquid directly or by actuating the membrane valve [13,14]. However, few works have been reported on the optofluidic devices which combine optics with the gas phase microfluidics. Very recently a pneumatically tunable optofluidic dye laser has been reported in which a microchannel based tunable air-gap etalon can be adjusted by air pressure [15]. Since the air pressure has been extensively utilized to manipulate both the liquid and optical elements on a chip, measurement of the air pressure and flow becomes desirable especially for local measurement inside the microfluidic chip.

In this work, we demonstrate an optical interferometric air pressure sensor and flow meter based on an air circulating optofluidic chip. Different from the MEMS (Microelectronic and Microelectromechanical Systems) based pressure or flow sensors which require sophisticated fabrication process with silicon [16,17], this optofluidic sensor was defined on a polymer chip with soft lithography and the measurement was done by imaging the interference pattern from the chip. This sensor can be simply fabricated with low cost.

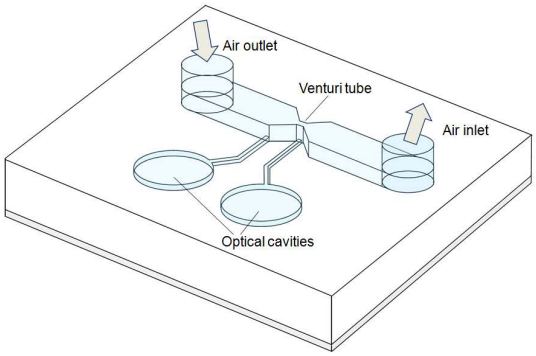

Fig. 1. The structure of optical chip including the microfluidic channel and optical cavities.

The chip structure is illustrated in Fig. 1. It consists of a structured Polydimethylsiloxane (PDMS) polymer layer bonded onto a rigid glass substrate. The structure inside the chip can be divided into two parts: the microfluidic channel and two separate optical cavities. The air flows in the main microfluidic channel. While in the channel middle part there exists a slit type Venturi tube for differential pressure based air flow measurement. Due to the elasticity of the polymer, the polymer optical cavities can be deformed by the local air pressure. Upon illuminating by monochromatic light, a Newton's ring pattern was formed in the cavities. By imaging and analyzing this interference pattern we can calculate the air pressure and hence the flow rate.

#129100 - $15.00 USD Received 27 May 2010; revised 8 Jul 2010; accepted 13 Jul 2010; published 22 Jul 2010

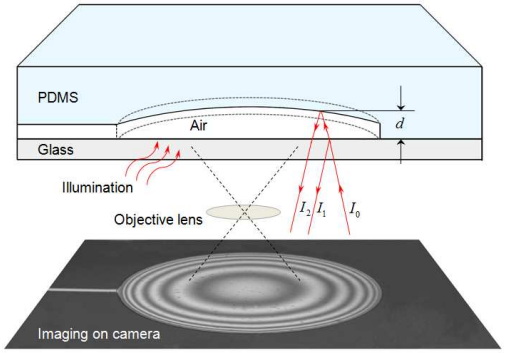

Fig. 2. The cross-section view and working principle of the optical cavity. Bottom picture shows the corresponding interference image on microscope.

The cross section of the optical cavity for pressure sensing is shown in Fig. 2. The top PDMS layer has a round chamber structure with flat inner surface. A thin air gap is formed between the PDMS chamber and glass substrate. Thanks to the flexibility of the PDMS, after filling with compressed air, the PDMS surface in the cavity was deflected into a curvature depending on the pressure value (all pressure here means the relative pressure to the atmosphere). When the cavity is illuminated by a coherent monochromatic light, the reflected light from the two inner surfaces of the cavity can interfere with each other constructively or destructively depending on the gap size. Thus the resulting total reflection intensity can be expressed as:

$$I = I_1 + I_2 + 2\sqrt{I_1 I_2}\cos\left(\frac{4d\pi}{\lambda} + \pi\right), \tag{1}$$

where I_1 and I_2 are the reflection intensity from the PDMS-air interface and air-glass interface respectively; d is the local air gap size; λ is the wavelength of the illuminating light. Due to the low reflectivity (< 4%) of these two interfaces, I_1 and I_2 have very close values hence resulting in good contrast of the interference pattern. Multiple reflections can be neglected in this model. As the PDMS/air interface will be deformed to a dome shape upon applying air pressure, the cavity generates multiple concentric ring interference fringes, similar to the Newton ring pattern.

Figure 3 shows the measuring principle of the air flow meter which is based on Venturi effect on a planar microfluidic Venturi tube. The Venturi tube is a section of the channels with a tapered entrance and a straight throat. As the fluid passes through the throat, the velocity increases. According to the Bernoulli's equation, the pressure drop across the constriction is proportional to the square of the flow rate. Thus the air flow rate Q can be expressed in a simplified form as [18]:

$$Q = k\sqrt{\Delta P \cdot \rho_1}, \tag{2}$$

where Q is the mass flow rate; $\Delta P = P_1 - P_2$ is the differential pressure; ρ_1 is the gas density before the entrance of the Venturi tube; k is a coefficient depending on the structure dimensions, environment temperature and other flow conditions. In this experiment, the temperature was assumed to be constant, so the air mass density ρ_1 before the taper entrance has $\rho_1 \propto P_1$ Thus the air mass flow rate can be also expressed as:

$$Q = k'\sqrt{\Delta P \cdot P_1}. \tag{3}$$

#129100 - $15.00 USD Received 27 May 2010; revised 8 Jul 2010; accepted 13 Jul 2010; published 22 Jul 2010

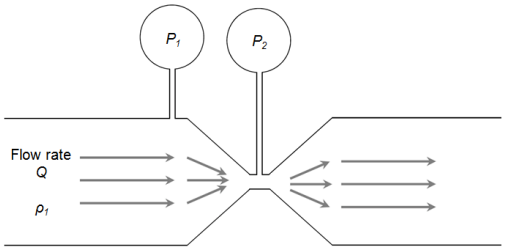

Fig. 3. The schematic of the Venturi tube for measuring the flow rate.

2. Fabrication

The structured PDMS layer was fabricated by soft-lithography in one step. It was replicated from a master mold which had double layers of structured negative photoresist SU-8 on a silicon wafer. The bottom layer of SU-8 had thickness of 15 um for defining the cavity structures. The cavity has a 300 µm diameter. After developing the first layer, a second layer of SU-8 was spun on top of it with a thickness of 50 um for defining the microfluidic channel. The main channel has width of 300 µm, and the width of the throat part is 50 µm. The PDMS was prepared by mixing the prepolymer component in 10:1 ratio (base: curing agent, Dow Corning Sylgard 184) and then baked in and oven at 80 degrees for 2 hours. Finally the PDMS layer was bonded on the glass substrate using oxygen plasma treatment.

3. Experiment and result

The chip was measured on a normal bright field microscope (Infinity Microscope and Mitutoyo M Plan Apo 5x objective) with a built-in beam splitter for illumination. The light source was based on a wideband light source (Dolan-Jenner PL-800 Illuminator) plus a laser line filter (Thorlabs, FL632.8-1) with a transmission linewidth of 1 nm. Instead of using the laser, this monochromatic light source was found to provide sufficient coherence for generating interference patterns and while suppressing almost completely the speckle noise. The image was recorded by a monocolor CCD camera. The air pressure was generated from a mechanical air pressure regulator (100-AB, Air Control Inc.) and calibrated with a digital pressure gauge (Omega DPG4000). The air flow was controlled by a digital mass flow controlled (Brooks Inc.).

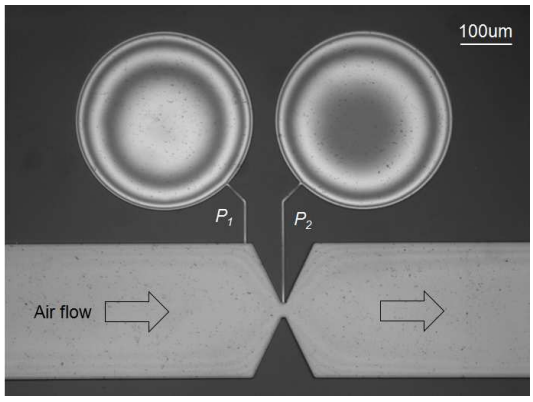

Fig. 4. An example image of the chip recorded on microscope.

#129100 - $15.00 USD Received 27 May 2010; revised 8 Jul 2010; accepted 13 Jul 2010; published 22 Jul 2010

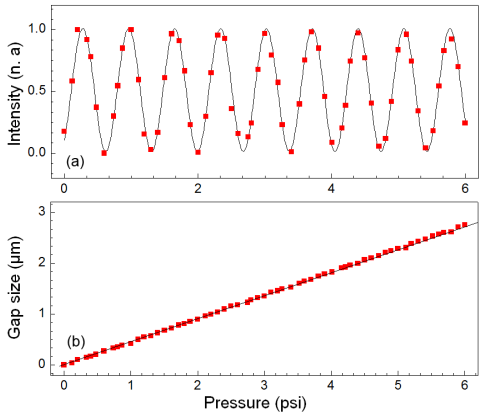

Fig. 5. The calibration results of the cavity P1. (a) The normalized average intensity at the center of the cavity versus the pressure. (b) The corresponding air gap size at the center versus the pressure.

Figure 4 shows an example image of the chip captured on the microscope. The cavities on the left and right correspond to the pressure sensor P_1 and P_2. The interference patterns consist of dark and bright co-centric rings which moved out from the center to the side as the pressure increased. Before the air flow measurements, these two pressure sensors were calibrated with the digital pressure gauge. Figure 5(a) shows the plot of the average intensity of the center in the left cavity P_1 versus the applied pressure, as denoted by the red solid squares. The scatter plot reveals a typical sinusoidal relationship which fits very well to a sine curve denoted by the black line. Based the Eq. (1), the increment of the air gap in the center can be calculated. The reconstructed result reveals nice linearity in the pressure range 0 - 6 psi as plotted by the air gap increment (red square dots) versus the applied pressure in Fig. 5(b). The sensitivity was calculated as 1.46 fringes per psi. As the left and right optical cavities are not exactly identical, two separate calibrations were done.

The digital mass flow meter was connected to a compress air source providing arbitrary air flow with predefined value. For the same air flow rate, different air pressure at the inlet of the chip was also tested by adjusting the resistance at the chip outlet. The interference images of the two cavities were recorded and analyzed according calibration results shown above. The result is shown in the Fig. 6. The plot shows the relation of the measured value of $\sqrt{P_1(P_1-P_2)}$ versus the flow rate (mg/second) which can fit Eq. (3) very well. Thus the value of the coefficient k' was calculated to be $0.377\ mg\cdot s^{-1}\cdot psi^{-1}$.

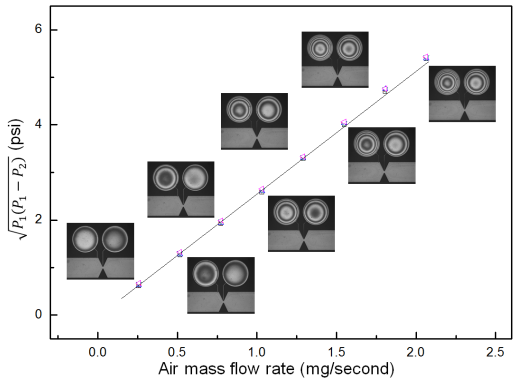

Fig. 6. The plot of the measured value of $\sqrt{P_1(P_1-P_2)}$ versus air mass flow rate. The inset pictures are the representative images recorded at each flow rate.

#129100 - $15.00 USD Received 27 May 2010; revised 8 Jul 2010; accepted 13 Jul 2010; published 22 Jul 2010

At the same flow rate, the values of $\sqrt{P_1(P_1-P_2)}$ (shown as different shapes on graph) give a slight deviation corresponding to different pressure condition at the inlet. Figure 7 illustrates the dependence of the measurement error versus different inlet pressure at certain flow rate. Here the measurement error is the differential value between the calculated value from Eq. (3) and the setting value of the digital mass flow controller.

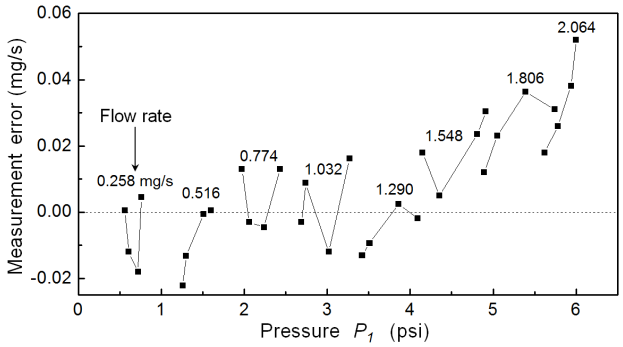

Fig. 7. The plot of the measurement error versus different inlet pressure at each flow rate.

For a given flow rate, the measurement errors seem random related to the variation of inlet pressures. This could be the result of the inaccuracy from the pressure sensing. For different flow rates, the measurement error has a tendency to increase monotonically with the flow rate. Such deviation was estimated to relate to the inaccuracy of Eq. (3) or the deformation of the microfluidic channel or another more complicated effect. However, this air flow meter still provides satisfied accuracy which is below ± 3% at full scale of 2 mg/s. The accuracy and dynamic range of this device are mainly limited by the mechanical properties of the PDMS. Firstly, the shape memory effect of PDMS is the main factor restricting the accuracy of pressure measurement; secondly, for high pressure and large flow rate, there is a slight deformation in the venture channel which can also induce errors.

4. Conclusion

In conclusion, we have demonstrated an optofluidic chip for simultaneously measuring the microfluidic air pressure and the flow rate through imaging. Both the microfluidic and optical structures were fabricated by soft-lithography on a polymer chip in a single step. Compared to the conventional miniature air pressure sensor or air flow meter which relies on complex MEMS fabrication process [17], this polymer based optofluidic air flow sensing chip can be made in mass production with very low cost. More importantly, as being compatible with the normal microfluidic in terms of fabrication and characterization [14], this device can be easily integrated into a lab-on-a-chip system for in situ measuring the air pressure and flow rate, Multipoint pressure or flow rate measurement are also feasible by simultaneously imaging the interference patterns on multiple cavities.

#129100 - $15.00 USD Received 27 May 2010; revised 8 Jul 2010; accepted 13 Jul 2010; published 22 Jul 2010